THE JOURNAL OF PHYSICAL CHEMISTRY C

ARTICLE

pubs.acs.org/JPCC

Influence of Donor Groups of Organic D−π−A Dyes on Open-Circuit Voltage in Solid-State Dye-Sensitized Solar Cells

Amalie Dualeh,[†] Filippo De Angelis,[*,‡] Simona Fantacci,[‡] Thomas Moehl,[†] Chenyi Yi,[†] Florian Kessler,[†] Etienne Baranoff,[†] Mohammad K. Nazeeruddin,[*,†] and Michael Grätzel[*,†]

[†]Laboratoire de Photoniques et Interfaces, Institut des Sciences et Ingénierie Chimiques, École Polytechnique Fédérale de Lausanne (EPFL), CH-1015 Lausanne, Switzerland

[‡]Istituto CNR di Scienze e Tecnologie Molecolari, c/o Dipartimento di Chimica, Università di Perugia, I-06123, Perugia, Italy

Supporting Information

ABSTRACT: In solid-state dye-sensitized solar cells (ssDSCs), the poor pore filling of the mesoporous semiconductor and the short diffusion length of charge carriers in the hole-transport material (HTM) have limited the mesoscopic titania layer to a thickness of 2−3 μm. To increase the amount of light harvested by ssDSCs, organic dyes with high molar extinction coefficients are of great importance and have been the focus of intensive research. Here we investigate ssDSCs using an organic D−π−A dye, coded Y123, and 2,2′,7,7′-tetrakis(*N*,*N*-di-*p*-methoxyphenylamine)-9,9′-spirobifluorene as a hole-transport material, exhibiting 934 mV open-circuit potential and 6.9% efficiency at standard solar conditions (AM1.5G, 100 mW cm^{-2}), which is a significant improvement compared to the analogue dyes C218, C220, and JK2 (V_{oc} values of 795, 781, and 914 mV, respectively). An upward shift in the conduction band edge was observed from photovoltage transient decay and impedance spectroscopy measurements for devices sensitized with Y123 and JK2 dyes compared to the device using C220 as sensitizer, in agreement with the high photovoltage response of the corresponding ssDSCs. This work highlights the importance of the interaction between the HTM and the dye-sensitized TiO_2 surface for the design of ssDSCs.

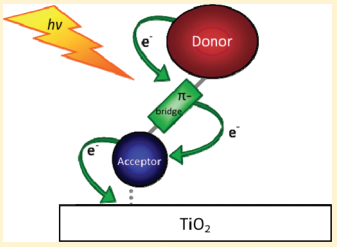

INTRODUCTION

Dye-sensitized solar cells (DSCs) have become an attractive candidate as an alternative source of renewable energy. DSCs mimic the process of photosynthesis, where a light-absorbing dye adsorbed onto a mesoporous semiconductor (TiO_2) takes the role of chlorophyll. Power conversion efficiencies (PCEs) close to 12% have been obtained with DSCs utilizing liquid electrolytes.[1] In solid-state DSCs (ssDSCs) the liquid electrolyte is replaced by a solid hole-transport material (HTM) to circumvent leakage problems associated with volatile solvents. Furthermore, this aims to improve the long-term stability as liquid based DSCs may suffer from corrosion of the metal contacts. ssDSCs offer the advantage in terms of large scale processability over their liquid based counterparts and are attractive in the realization of the roll-to-roll production of flexible photovoltaic devices. While extensive research has been conducted on different HTMs,[2−5] the amorphous organic semiconductor 2,2′,7,7′-tetrakis(*N*,*N*-di-*p*-methoxyphenylamine)-9,9′-spirobifluorene (spiro-MeOTAD, Figure 1) has remained the material of choice for high efficiency devices since it was first reported in 1998 by Bach et al.[6] In order to improve ssDSC operation, it is important to understand the manner in which this HTM interacts with the sensitized TiO_2 surface.

However, the advantages of ssDSCs are accompanied by disadvantages. Due to incomplete pore filling of the mesoporous TiO_2 electrode with the spiro-MeOTAD and the short diffusion length associated with it, ssDSCs are limited to very thin titania layers.[2,7,8] Consequently, dyes with high molar extinction coefficients are necessary to achieve sufficient light harvesting for reaching high power conversion efficiencies (PCEs).[9,10] This recent movement away from organometallic dye complexes allows for thinner device designs and a more discrete HTM−dye interface.

The open-circuit voltage (V_{oc}) of ssDSCs is determined primarily by the difference between the quasi Fermi level of the conduction band electrons in the semiconductor, TiO_2, under illumination and the oxidation potential of the HTM. The value of the oxidation potential of spiro-MeOTAD in solution has been found to be 0.72 V versus normal hydrogen electrode (NHE).[11] Assuming a value of −0.5 V vs NHE for the TiO_2 conduction band (CB) edge,[12] one is limited to the theoretical V_{oc} value of about 1.2 V. Variations in the V_{oc} can be caused by an increased concentration of holes (e.g., due to doping), resulting in a lower Fermi level in the HTM. Alternatively, the V_{oc} can be affected by the electron density in the semiconductor and/or by an upward shift of the semiconductor CB edge.[13] In this study the devices were all fabricated following the same doping procedure (using a Co(III) complex, tris(2-(1*H*-pyrazol-1-yl)pyridine)cobalt(III) tris(hexafluorophosphate)[11] as a p-type dopant) and hence it is assumed that any shift in the HTM Fermi level is not of significant value.

Solid-state dye-sensitized solar cells were fabricated using spiro-MeOTAD as a hole conductor and the high molar extinction coefficient organic D−π−A dyes[9,14−16] coded JK2, C218, C220,

Received: October 15, 2011
Revised: December 7, 2011
Published: December 07, 2011

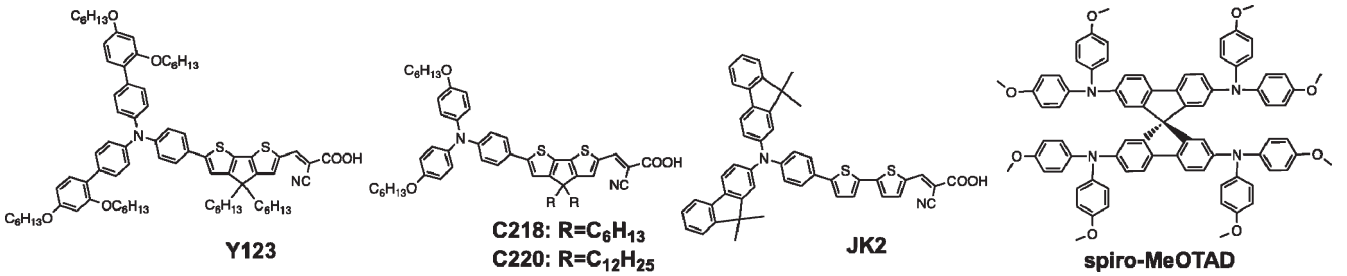

Figure 1. Molecular structures of Y123, C218, C220, JK2, and spiro-MeOTAD.

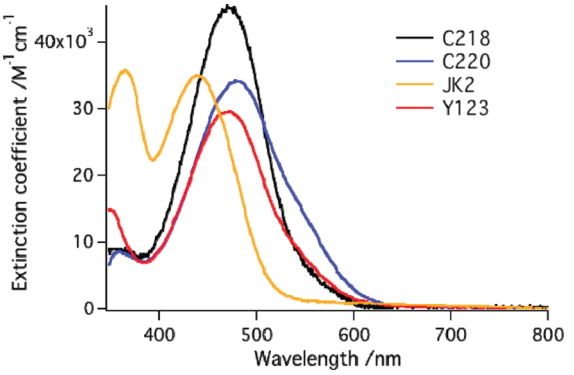

Figure 2. UV−vis spectra of C218, C220, JK2, and Y123 in 1:1 solvent mixture of acetonitrile and *tert*-butyl alcohol.

and Y123 (Figure 1), as sensitizers. In combination with a Co^{III}/Co^{II} redox electrolyte, liquid DSCs with PCEs of 9.6% have been realized with Y123.[16] Its analogue, C220, has been reported as a best performing dye in ssDSCs,[9] while JK2 achieved the highest V_{oc} of over 1 V in ssDSCs, albeit at relatively low photocurrents.[14] In this study we assess the role of the dye in determining the open-circuit voltage of ssDSCs.

RESULTS AND DISCUSSION

The UV−vis spectra of C218, C220, JK2, and Y123 in a 1:1 solvent mixture of acetonitrile and *tert*-butyl alcohol exhibit absorption maxima at 471, 481, 440, and 472 nm with molar absorption coefficients of 45 × 10^3, 34 × 10^3, 35 × 10^3, and 29 × 10^3 M^{-1} cm^{-1}, respectively (Figure 2).

The *J*−*V* characteristics of ssDSCs fabricated using the sensitizers JK2, C218, C220, and Y123 measured at 1 sun illumination under standard global AM1.5G conditions (100 mW cm^{-2}) are shown in Figure 3a with the corresponding photovoltaic (PV) parameters summarized in Table 1. The device using the Y123 dye gave an impressive efficiency of 6.9%, which can be attributed to the high V_{oc} of 934 mV and fill factor (FF) of 0.75. For devices made with JK2 and C220 we found open-circuit potential, V_{oc}, short-circuit current density, J_{sc}, and fill factor, FF, values of 914 and 781 mV, 8.9 and 11.5 mA cm^{-2}, and 0.60 and 0.64, respectively, yielding PCEs of 4.9 and 5.7%, respectively. The performance of devices with C218 is similar to that of devices with C220. The FFs of devices with Y123 were observed to be consistently higher. Previous studies[5] have shown that higher rates of recombination lead to poor FFs, which suggests that JK2, C220, and C218 suffer from faster recombination.

The increase in J_{sc} with the order JK2 < Y123 < C220 < C218 arises from the improved light harvesting ability of the dyes which

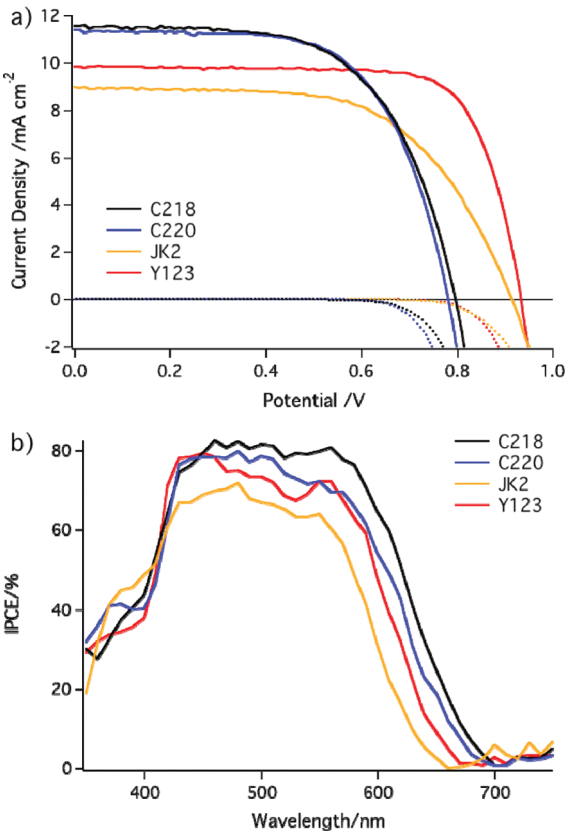

Figure 3. (a) *J*−*V* characteristics of C218, C220, JK2, and Y123 sensitized ssDSCs measured under dark (dashed lines) and 100 mW cm^{-2} (solid lines) AM1.5G solar intensity. (b) Corresponding IPCE spectra as a function of monochromatic wavelength.

Table 1. Photovoltaic Parameters Determined from *J*−*V* Measurements for ssDSCs Using C218, C220, JK2, and Y123 Measured under Simulated AM1.5G Solar Irradiance (100 mW cm^{-2})[a]

dye	V_{oc}/mV	J_{sc}/mA cm^{-2}	FF	PCE/%
C218	796	11.6	0.61	5.6
C220	781	11.5	0.64	5.7
JK2	914	8.9	0.60	4.9
Y123	934	9.8	0.75	6.9

[a] All devices were masked to achieve an illuminated active area of 0.2025 cm^{-2}.

is evident in the incident-photon-to-current conversion efficiency (IPCE) spectra (Figure 3b). The similar shapes of the

dx.doi.org/10.1021/jp209691e |*J. Phys. Chem. C* 2012, 116, 1572–1578

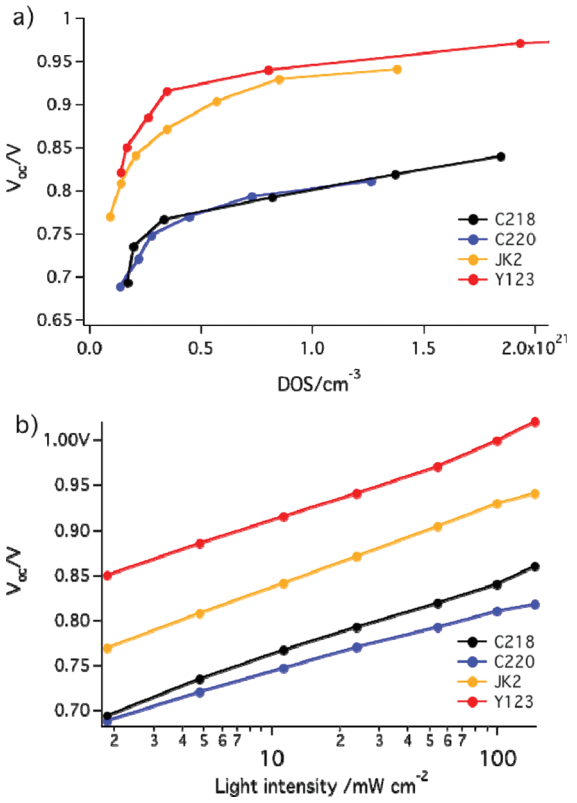

Figure 4. V_{oc} dependence on (a) DOS and (b) light intensity determined from transient measurements of C218, C220, JK2, and Y123 sensitized ssDSCs.

IPCE spectra reflect the light absorption qualities of the dyes inferred from the absorption spectra and lie between 70 and 80% from 450 to 570 nm, with the maximum achieved at the plateau for C218, followed by C220, Y123, and JK2. Additionally, the IPCE spectra are strongest in the red regions for C218 and weakest for JK2. The projected current density values calculated by integration of the IPCE spectra over the AM1.5G standard solar emission spectra are 11.5, 10.8, 9.1, and 10.1 mA cm^{-2} for C218, C220, JK2, and Y123, respectively. This reflects the difference in the IPCE spectra and is in good agreement with the J_{sc} values obtained from the standard PV characterizations. Especially in the case of JK2, the lower light harvesting abilities of the dye lead to lower J_{sc} and thus lower PCE. However, the J_{sc} is also affected by the adsorption capabilities of the dyes which determines their surface coverage and is examined in more detail below. Furthermore, the position of the CB edge influences the injection efficiency and consequently also the photocurrent.

One of the key components of dye-sensitized solar cells is the nanocrystalline TiO_2 film. The chemical capacitance is a measure of the number of charges that can be stored in the traps within the TiO_2 nanoparticles and at their interface with the HTM.[17−19] Systems made up of nanoparticulate TiO_2 layers contain considerably higher concentrations of electrons in traps than in the CB.[20] The chemical capacitance at a given voltage is proportional to the density of trap states (DOS), which can be calculated using[21]

$$\mathrm{DOS} = (6.24 \times 10^{18})\frac{C}{d(1-p)} \qquad (1)$$

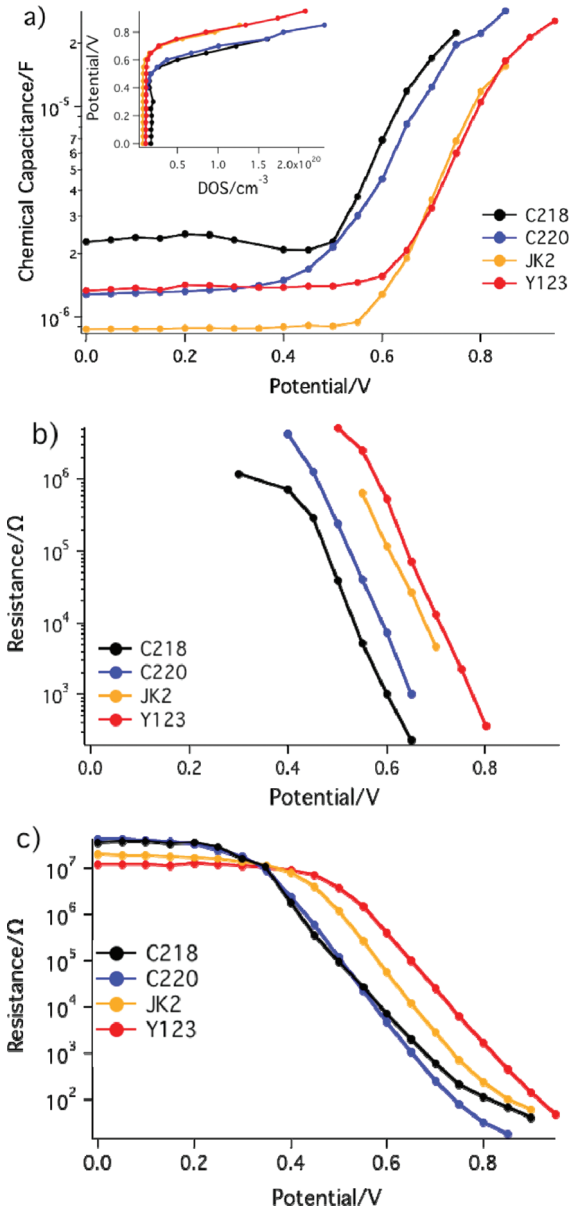

Figure 5. (a) Chemical capacitance, (b) transport resistance, and (c) recombination resistance for C218, C220, JK2, and Y123 sensitized ssDSCs. The inset in (a) shows the potential as a function of DOS calculated from the chemical capacitance for the same devices.

where C is the capacitance per unit area, d is the thickness of the TiO_2 film, and p is the porosity. The conversion factor represents the number of electrons per coulomb.

Transient photovoltage and photocurrent were measured to study the internal electrical parameters of the devices.[5] The ssDSCs were held at constant V_{oc} and exposed to a small perturbation by a short light pulse. The resulting response of the system was monitored at different light intensities. The transient photocurrent data were used to calculate the capacitance at V_{oc}[21,22] from which the DOS was determined using eq 1 (Figure 4a). This shows a shift of 150 and 130 mV in the V_{oc} between Y123 or JK2 and C220 sensitized devices, respectively. These values are in good agreement with the difference observed in V_{oc}.

Figure 4b shows a plot of the V_{oc} as a function of the logarithm of the light intensity for the different devices. The slope obtained

dx.doi.org/10.1021/jp209691e |J. Phys. Chem. C 2012, 116, 1572–1578

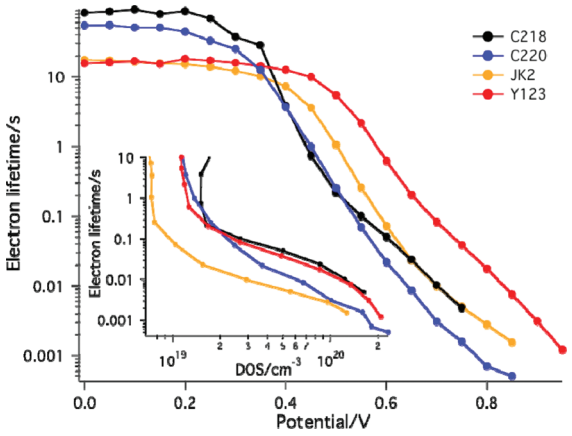

Figure 6. Electron lifetimes of C218, C220, JK2, and Y123 sensitized ssDSCs. The inset shows the electron lifetime against the DOS.

for C218, C220, JK2, and Y123 was found to be 86, 72, 90, and 80 mV dec^{-1} (diode ideality factor m of 1.4, 1.2, 1.5, and 1.3), respectively, indicating that these devices show similar deviations from ideal diode behavior.[23]

To further investigate the internal electrical characteristics of the ssDSCs, electrochemical impedance spectroscopy (IS) measurements were conducted in the dark. The transmission line model[24] was used to analyze the IS spectra, the results of which are presented in Figure 5. The transport resistance, R_t, and chemical capacity, C_μ, are respectively measures of the conductivity and the charge density of the nanostructured TiO_2 film. The charge transfer (also termed "recombination") resistance, R_r, accounts for the recombination current at the interface between the TiO_2 and the HTM. At low potentials, the TiO_2 acts as an insulator; thus both R_t and R_r are very large and the behavior is dominated by the interface between the HTM and the compact blocking TiO_2 underlayer. At higher potentials, the electron density in the mesoporous TiO_2 increases and thus the conductivity of the TiO_2 increases. This latter aspect is reflected in the exponential increase in the chemical capacity.[25]

The devices made with C218, C220, JK2, and Y123 show IS spectra with similar shapes. The shifts in the CB observed in the transient measurements are reflected in the chemical capacitance determined by IS (Figure 5a). This shows an upward shift in the CB of the TiO_2 of approximately 150 and 130 mV for devices using Y123 and JK2 relative to C220, respectively. C218 shows a small negative shift of approximately 30−40 mV compared to C220. This trend is also observed in the shifts in the transport resistances, R_t, respective to the potential (Figure 5b). These correspond to an upward shift of 150 and 100 mV for Y123 and JK2, respectively, relative to C220. In the case of C218, a downward shift of 50 mV relative to C220 is observed, which is also in good agreement with the chemical capacitance from IS.

The similar shifts in C_μ and R_t for Y123 and JK2 relative to C220 suggest that they have comparable DOSs and conductivities of the TiO_2. However, in the case of the recombination resistances R_r, the displacement with respect to the potential (Figure 5c) shows a significant difference (170 and 100 mV, respectively), indicating that JK2 has higher recombination. Furthermore, C218 and C220 show similar recombination resistances at the same applied potential. Taking into account the shift in the CB for these two dyes, this implies a higher recombination for C220 (see also inset of Figure 6).

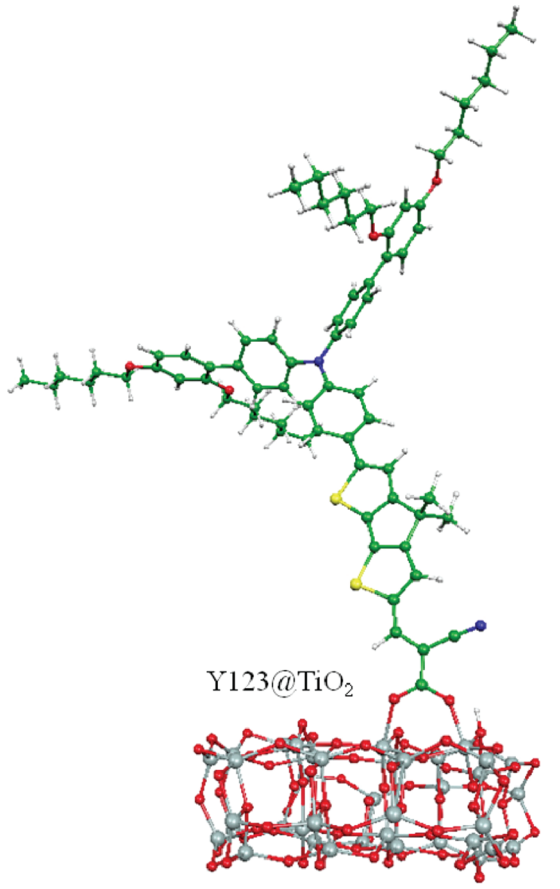

Figure 7. Calculated adsorption geometry for Y123 on TiO_2. The same adsorption mode is calculated for C220.

From these results the electron lifetime, τ_e, within the TiO_2 was determined using the following relationship:[24]

$$\tau_e = R_r C_\mu \quad (2)$$

The electron lifetime depends on the concentration of electrons in the CB, which in turn depends on the rate of trapping and detrapping of electrons in localized states within the band gap of the TiO_2. Thus the electron lifetime is strongly influenced by the applied voltage (Figure 6). At similar potentials it is apparent that the electron lifetime is longest for ssDSCs with Y123 and shortest for C220 resulting from a lower recombination resistance. The inset of Figure 6 shows the electron lifetime as a function of the DOS, thus allowing for comparison of the recombination rates at the same electron density. Shorter electron lifetimes are measured for JK2 and C220 at similar potentials, reflecting the higher rates of recombination for these sensitizers.

The adsorption of dipolar molecules onto the TiO_2 surface has been shown to influence the position of the CB edge.[26] Studies examining such surface modification techniques have led to improvement of the V_{oc} of liquid DSCs.[27] Furthermore, the presence of dipoles on the surface has been shown to act as surface blocking layers, suppressing the dark current in ssDSCs and leading to a change in the band alignment at the sensitized semiconductor/HTM interface.[28] It is clear that the dipole moment of the adsorbed dye molecules has a strong effect on

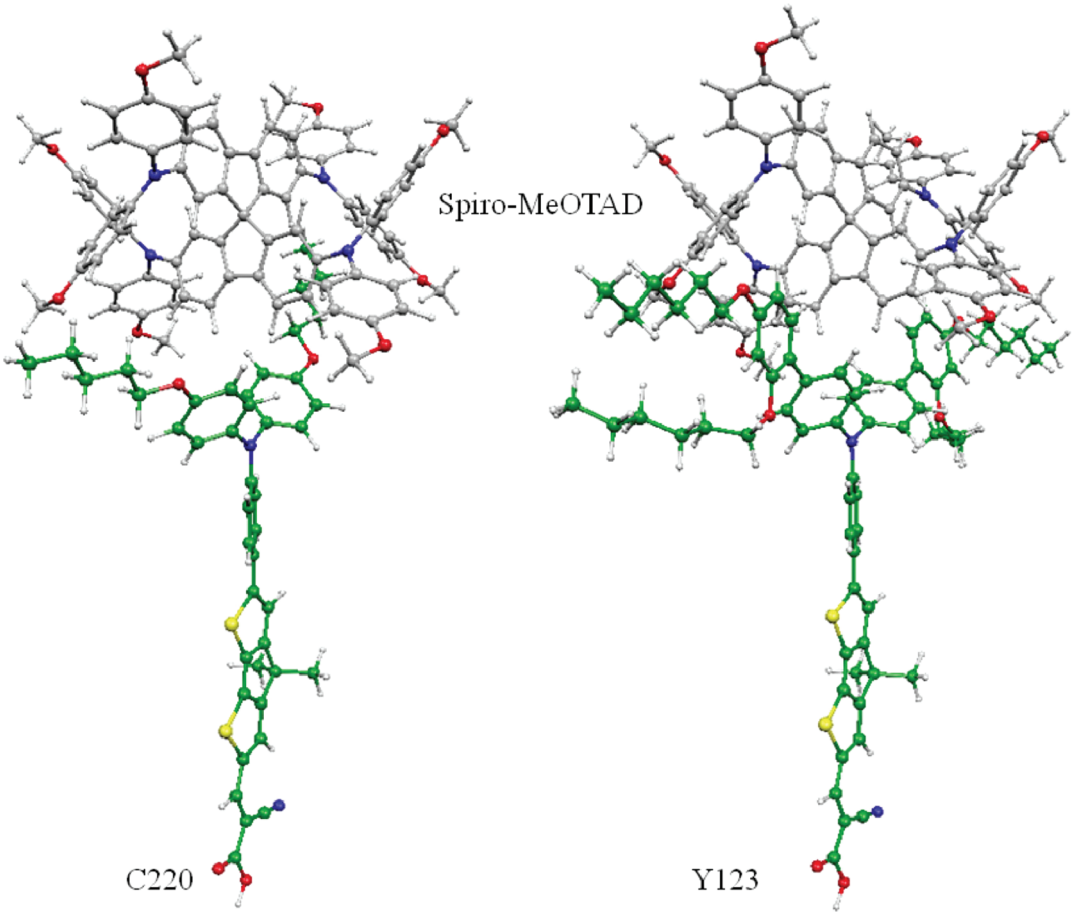

Figure 8. Optimized geometries of C220 and Y123 adducts with spiro-MeOTAD. Carbon atoms belonging to the spiro-MeOTAD molecule are displayed in gray for clarity.

the charge distribution and consequently influences the position of the semiconductor CB.

To gain insight into the electronic and optical properties of the investigated dyes and their interaction with the TiO_2 semiconductor and the spiro-MeOTAD hole conductor, DFT/TDDFT calculations were performed on the C220, JK2, and Y123 dyes. The optimized geometries of the three dyes are reported in Figure S1 of the Supporting Information. C220 and Y123 show a planar arrangement of the conjugated phenyl−CPDT−cyanoacrylic acid moiety, while the two aromatic moieties bound to the nitrogen donor are displaced out of plane to minimize steric repulsion.

It can be noticed from an isodensity plot of the highest occupied molecular orbitals (HOMOs) and lowest unoccupied molecular orbitals (LUMOs) for C220 and Y123 that they share a common electronic structure (see Figure S2 in Supporting Information). They display the typical HOMO−LUMO pattern characteristic of these push−pull dyes, whereby the HOMO is mainly localized on the donor and bridge portion of the molecules, while the LUMO is mainly localized on the bridge and on the anchoring/acceptor moiety.

The lowest TDDFT transition energies (see Supporting Information) for the protonated (deprotonated) C220, JK2, and Y123 dyes in ethanol solution are calculated at 521 (456), 507 (441), and 519 (451) nm. These lowest transitions are originated in all cases from intense HOMO−LUMO excitations. As previously observed, a blue shift of the absorption is found upon deprotonation of the terminal carboxylic group[29] and is observed in the corresponding experimental data (Figure 2). Overall, the calculated excitation energies for the deprotonated dyes are in good agreement with experimental absorption maxima (481, 440, and 472 nm for C220, JK2, and Y123, respectively), with maximum deviations within 0.14 eV. Furthermore, our calculations reproduce the absorption maxima trend, showing a slight red shift from Y123 to C220 and a substantial blue shift from the latter to JK2.

The total dipole moments for C220 and Y123 are calculated to be 10.6 and 11.5 D, respectively, and they are found to be oriented along the main push−pull molecular axis, pointing from the cyanoacrylic acceptor to the N-substituted donor.

To evaluate the dipole component normal to the TiO_2 semiconductor surface, which may be responsible for the observed shifts in TiO_2 CB, the geometry of Y123 on the $(TiO_2)_{38}$ cluster was optimized. Similar to what was previously reported for the similar JK2 dye,[14] an analogous adsorption geometry was found for Y123, with a dissociative bidentate adsorption mode and a proton transferred to the TiO_2 surface (Figure 7).

From the calculated adsorption geometry, dipole components normal to the TiO_2 surface of 8.8 and 8.6 D for Y123 and C220, respectively, were calculated. Thus the two dyes have similar dipole moments and adsorption modes, so if a dipole shift of the TiO_2 CB is at work, it is likely related to varying dye coverage. Dye desorption experiments were conducted to determine the extents of dye loading of the different sensitizers. In the case of Y123 the dye coverage was found to be 23% higher in

comparison to C220 (2.80×10^{-6} and 3.45×10^{-6} mol m^{-2} for C220 and Y123, respectively). The longer dodecyl alkyl chains of C220 reduce the close packing of the molecules on the surface as well as increase the solubility in solution. Employing the calculated dipole moments and the experimentally available dye coverages, a TiO_2 CB upshift of ca. 100 mV for Y123 compared to C220 was calculated which is comparable to the experimental values. Considering the similar adsorption mode (see Figure S3 in Supporting Information) and dipole moment calculated for JK2 (previously reported as 7.7 D[14]) along with the measured dye coverage (21% higher relative to C220), a similar shift for JK2 is predicted, in line with the experimental findings.

The dye coverages alone, however, do not provide an explanation for the roughly same conduction band potential observed for C220 and C218 (the latter having a dye coverage of 35% higher relative to C220), which differ only by the length of the alkyl chain on the CPDT moiety, compared to Y123 which has the same alkyl chain as C218. An additional difference is therefore present due to the different donor groups in C220/C218 and Y123. Since the dye donor group is possibly responsible for the dye interaction with the spiro-MeOTAD hole conductor, the acceptor being firmly anchored to the TiO_2 surface, we investigated the interaction of the C220 (or C218) and Y123 dyes with a spiro-MeOTAD molecule and calculated the corresponding dye/spiro adducts reported in Figure 8.

The calculated interaction geometries between C220 and Y123 with spiro-MeOTAD are rather similar, with calculated distances between the dye N-donor and the spiro carbon of 8.74 and 8.81 Å, respectively. The calculated MP2 interaction energies, however, are substantially different for the two dyes, with C220 showing an adduct formation energy of 14.1 kcal mol^{-1}, while this quantity reduces to 9.5 kcal mol^{-1} for Y123. Thus, by virtue of the more bulky donor group of Y123, a reduced interaction energy with spiro-MeOTAD is computed for this dye compared to C220. For the JK2 dye we expect a somehow reduced interaction with spiro-MeOTAD compared to C220, similar to that calculated for Y123, because of the bulky donor substituents carried by this dye.

We speculate here that a strong dye/spiro interaction might cause the spiro-MeOTAD molecules to bind strongly to the dye donor groups rather than binding among themselves to form a well-dispersed film, increasing the recombination between injected electrons and the oxidized spiro-MeOTAD and leading to a reduced lifetime for C220 and C218 compared to Y123 and JK2. It is also possible that the higher interaction energy beteween C220 and spiro-MeOTAD partially compensates the net dipole moment of the sensitizer, which is not the case for Y123, resulting in the shift of the CB edge.

CONCLUSIONS

This work presented the photovoltaic performance of organic D−π−A dyes in ssDSCs and explored the origin of the difference in the open-circuit potential. The DOSs derived from photovoltage transient decay and impedance spectroscopy measurements are in good agreement with the photovoltaic performance and show that the increase in V_{oc} can be attributed to an upward shift of the CB of the TiO_2 for Y123 and JK2 relative to C220 or C218. The presence and length of the alkyl substituents on the bridge segment of the dye molecules play an important role in dye surface coverage, which influences the net surface dipole effect but does not solely account for the CB shift. The different donor groups, having different extents of interaction with the HTM, lead to different charge transfer rates at the spiro-MeOTAD/dye interface. Calculated interaction energies between the dyes and spiro-MeOTAD suggest that different donor groups influence the strength of the interaction with the solid HTM when it is deposited out of solution by spin coating, thus maybe affecting the transport properties of the spiro-MeOTAD. The upward CB shift of Y123 relative to C220 or C218 is believed to originate from a contribution of the higher net surface dipole moment effect arising from higher dye coverage and from a lower spiro/dye interaction energy due to the specific nature of its donor group. In the case of C220, the strong spiro/dye interaction appears to lead to a higher rate of recombination and partial compensation of the surface dipole moment by the HTM. The interaction between the HTM and the TiO_2-adsorbed dye is believed to influence the net surface dipole moment as well as the charge transfer properties, and thus is an important parameter to consider in ssDSC operation. This work shows the importance of carefully designing the individual components of new dyes and characterizing their interactions with the HTM in order to reach high efficiencies in ssDSCs.

ASSOCIATED CONTENT

Supporting Information. Experimental details on device fabrication and characterization. Computational details, optimized geometries, molecular orbitals and TDDFT transition energies. This material is available free of charge via the Internet at http://pubs.acs.org.

AUTHOR INFORMATION

Corresponding Author

*E-mail: michael.graetzel@epfl.ch (M.G.); filippo@thch.unipg.it (F.D.); mdkhaja.nazeeruddin@epfl.ch (M.K.N).

ACKNOWLEDGMENT

The authors thank Prof. Jaejung Ko for providing the JK2 and Prof. Peng Wang for providing the C220 and C218 sensitizers. This work was funded by the European Community's Seventh Framework Programme (FP7/2007-2013) under the "ORION" grant agreement no. NMP-229036, "SANS" agreement no. 246124, and "ESCORT" agreement no. ENERGY-261920. M.K.N. thanks the World Class University program, Photovoltaic Materials, Department of Material Chemistry, Korea University, Chungnam, 339-700, Korea, funded by the Ministry of Education, Science and Technology through the National Research Foundation of Korea (No. R31-2008-000-10035-0). F.D. and S.F. thank Fondazione Istituto Italiano di Tecnologia, and Project SEED 2009 "HELYOS" for financial support. M.G. thanks the ERC for providing an Advanced Research Grant for the MESOLIGHT project.

REFERENCES

(1) Chen, C. Y.; Wang, M. K.; Li, J. Y.; Pootrakulchote, N.; Alibabaei, L.; Cevey-Ha, L.; Decoppet, J. D.; Tsai, J. H.; Grätzel, C.; Wu, C. G.; Zakeeruddin, S. M.; Grätzel, M. *ACS Nano* **2009**, *3*, 3103–3109.

(2) Schmidt-Mende, L.; Grätzel, M. *Thin Solid Films* **2006**, *500*, 296–301.

(3) Kroeze, J. E.; Hirata, N.; Schmidt-Mende, L.; Orizu, C.; Ogier, S. D.; Carr, K.; Grätzel, M.; Durrant, J. R. *Adv. Funct. Mater.* **2006**, *16*, 1832–1838.

(4) O'Regan, B. C.; Schwartz, D. T. *Chem. Mater.* **1998**, *10*, 1501–1509.
(5) O'Regan, B. C.; Lenzmann, F. *J. Phys. Chem. B* **2004**, *108*, 4342–4350.
(6) Bach, U.; Lupo, D.; Comte, P.; Moser, J. E.; Weissortel, F.; Salbeck, J.; Spreitzer, H.; Grätzel, M. *Nature* **1998**, *395*, 583–585.
(7) Snaith, H. J.; Humphry-Baker, R.; Chen, P.; Cesar, I.; Zakeeruddin, S. M.; Grätzel, M. *Nanotechnology* **2008**, *19*, No. 424003.
(8) Snaith, H. J.; Grätzel, M. *Appl. Phys. Lett.* **2006**, *89*, No. 262114.
(9) Cai, N.; Moon, S.-J.; Cevey-Ha, L.; Moehl, T.; Humphry-Baker, R.; Wang, P.; Zakeeruddin, S. M.; Grätzel, M. *Nano Lett.* **2011**, *11*, 1452–1456.
(10) Moon, S.-J.; Yum, J.-H.; Humphry-Baker, R.; Karlsson, K. M.; Hagberg, D. P.; Marinado, T.; Hagfeldt, A.; Sun, L.; Grätzel, M.; Nazeeruddin, M. K. *J. Phys. Chem. C* **2009**, *113*, 16816–16820.
(11) Burschka, J.; Dualeh, A.; Kessler, F.; Baranoff, E.; Cevey-Ha, N.-L.; Yi, C.; Nazeeruddin, M. K.; Grätzel, M. *J. Am. Chem. Soc.* **2011**, *133*, 18042–18045.
(12) De Angelis, F.; Fantacci, S.; Selloni, A. *Nanotechnology* **2008**, *19*, No. 424002.
(13) Bisquert, J. *Phys. Chem. Chem. Phys.* **2008**, *10*, 49–72.
(14) Chen, P.; Yum, J. H.; Angelis, F. D.; Mosconi, E.; Fantacci, S.; Moon, S.-J.; Baker, R. H.; Ko, J.; Nazeeruddin, M. K.; Grätzel, M. *Nano Lett.* **2009**, *9*, 2487–2492.
(15) Li, R. Z.; Liu, J. Y.; Cai, N.; Zhang, M.; Wang, P. *J. Phys. Chem. B* **2010**, *114*, 4461–4464.
(16) Tsao, H. N.; Yi, C.; Moehl, T.; Yum, J.-H.; Zakeeruddin, S. M.; Nazeeruddin, M. K.; Grätzel, M. *ChemSusChem* **2011**, *4*, 591–594.
(17) Fabregat-Santiago, F.; Garcia-Belmonte, G.; Bisquert, J.; Zaban, A.; Salvador, P. *J. Phys. Chem. B* **2002**, *106*, 334–339.
(18) Willis, R. L.; Olson, C.; O'Regan, B.; Lutz, T.; Nelson, J.; Durrant, J. R. *J. Phys. Chem. B* **2002**, *106*, 7605–7613.
(19) Peter, L. M.; Duffy, N. W.; Wang, R. L.; Wijayantha, K. G. U. *J. Electroanal. Chem.* **2002**, *524*, 127–136.
(20) van de Lagemaat, J.; Frank, A. J. *J. Phys. Chem. B* **2000**, *104*, 4292–4294.
(21) O'Regan, B. C.; Scully, S.; Mayer, A. C.; Palomares, E.; Durrant, J. *J. Phys. Chem. B* **2005**, *109*, 4616–4623.
(22) Sommeling, P. M.; O'Regan, B. C.; Haswell, R. R.; Smit, H. J. P.; Bakker, N. J.; Smits, J. J. T.; Kroon, J. M.; van Roosmalen, J. A. M. *J. Phys. Chem. B* **2006**, *110*, 19191–19197.
(23) Cameron, P. J.; Peter, L. M. *J. Phys. Chem. B* **2005**, *109*, 7392–7398.
(24) Bisquert, J.; Garcia-Belmonte, G.; Fabregat-Santiago, F.; Compte, A. *Electrochem. Commun.* **1999**, *1*, 429.
(25) Bisquert, J.; Fabregat-Santiago, F. In *Dye-sensitized Solar Cells*; Kalyanasundaram, K., Ed.; CRC Press: Lausanne, Switzerland, 2010.
(26) Kruger, J.; Bach, U.; Grätzel, M. *Adv. Mater.* **2000**, *12*, 447–451.
(27) Rühle, S.; Greenshtein, M.; Chen, S. G.; Merson, A.; Pizem, H.; Sukenik, C. S.; Cahen, D.; Zaban, A. *J. Phys. Chem. B* **2005**, *109*, 18907–18913.
(28) Kruger, J.; Plass, R.; Cevey, L.; Piccirelli, M.; Grätzel, M.; Bach, U. *Appl. Phys. Lett.* **2001**, *79*, 2085–2087.
(29) Pastore, M.; Mosconi, E.; De Angelis, F.; Grätzel, M. *J. Phys. Chem. C* **2010**, *114*, 7205–7212.